MICROSCOPY

Microscopy, 2020, 401–407
doi: 10.1093/jmicro/dfaa031
Advance Access Publication Date: 11 June 2020

Technical Report

Kinetic analysis of the intracellular processing of siRNAs by confocal microscopy

Daniel Vocelle[1], Olivia M. Chesniak[2], Milton R. Smith III[2], Christina Chan[1,3] and S. Patrick Walton[1,*]

[1]Department of Chemical Engineering and Materials Science, Michigan State University, 428 S Shaw Lane, East Lansing, MI 48824, USA, [2]Department of Chemistry, Michigan State University, 578 S Shaw Lane, East Lansing, MI 48824, USA, and [3]Department of Biochemistry and Molecular Biology, Michigan State University, 603 Wilson Road, East Lansing, MI 48824, USA

*To whom correspondence should be addressed. E-mail: spwalton@msu.edu

Received 2 February 2020; Revised 20 May 2020; Accepted 7 June 2020

Abstract

Here, we describe a method for tracking intracellular processing of small interfering RNA (siRNA) containing complexes using automated microscopy controls and image acquisition to minimize user effort and time. This technique uses fluorescence colocalization to monitor dual-labeled fluorescent siRNAs delivered by silica nanoparticles in different intracellular locations, including the early/late endosomes, fast/slow recycling endosomes, lysosomes and the endoplasmic reticulum. Combining the temporal association of siRNAs with each intracellular location, we reconstructed the intracellular pathways used in siRNA processing, and demonstrate how these pathways vary based on the chemical composition of the delivery vehicle.

Key words: siRNA, confocal microscopy, intracellular trafficking, HeLa, delivery vehicles, kinetics

Introduction

Understanding the intracellular processing of small interfering RNA (siRNA) containing complexes is critical to the design of siRNA delivery vehicles. While siRNAs trafficked to the cytoplasm can be actively incorporated into the RNA interference (RNAi) pathway, endosomal recycling and endolysosomal retention can result in siRNAs being exocytosed or degraded [1,2]. It is estimated that $< 1\%$ of internalized siRNAs reach the cytoplasm [2]. Thus, to maximize siRNA activity, it is useful to design delivery vehicles to enhance the trafficking of siRNAs to the cytoplasm. However, it is unclear how to optimize delivery vehicle characteristics for optimal intracellular processing [3].

Confocal microscopy is the preferred method to study intracellular trafficking, as fluorescent colocalization analysis can quantify spatiotemporal biological interactions. However, it is currently considered labor intensive, requiring constant operator supervision to maintain well position, focal plane and cell viability over the duration of the experiment [4,5]. For experiments focused specifically on siRNA processing, several methods have been used to evaluate the processing of both guide and passenger siRNA strands [6–8]. However, researchers generally have to choose between using fixed cell images to identify the intracellular location of siRNAs or using live cell images to obtain kinetic information related to siRNA trafficking in a single intracellular location.

Here, we describe a method that overcomes these limitations allowing researchers to track the kinetics of siRNA trafficking across multiple intracellular locations. Our method uses automated multi-well fluorescence imaging of stable cell lines to increase the throughput of live-cell imaging and decrease the labor associated with image collection, while not sacrificing data quantity or quality. We applied our method to characterize the intracellular processing of siRNA-containing complexes and measure kinetic variations that arise from delivery by silica nanoparticles (sNPs) with different chemical compositions.

During the development of our assay, several points of automation were included to reduce operator intervention and improve the throughput of live-cell imaging. Long-term cell viability and

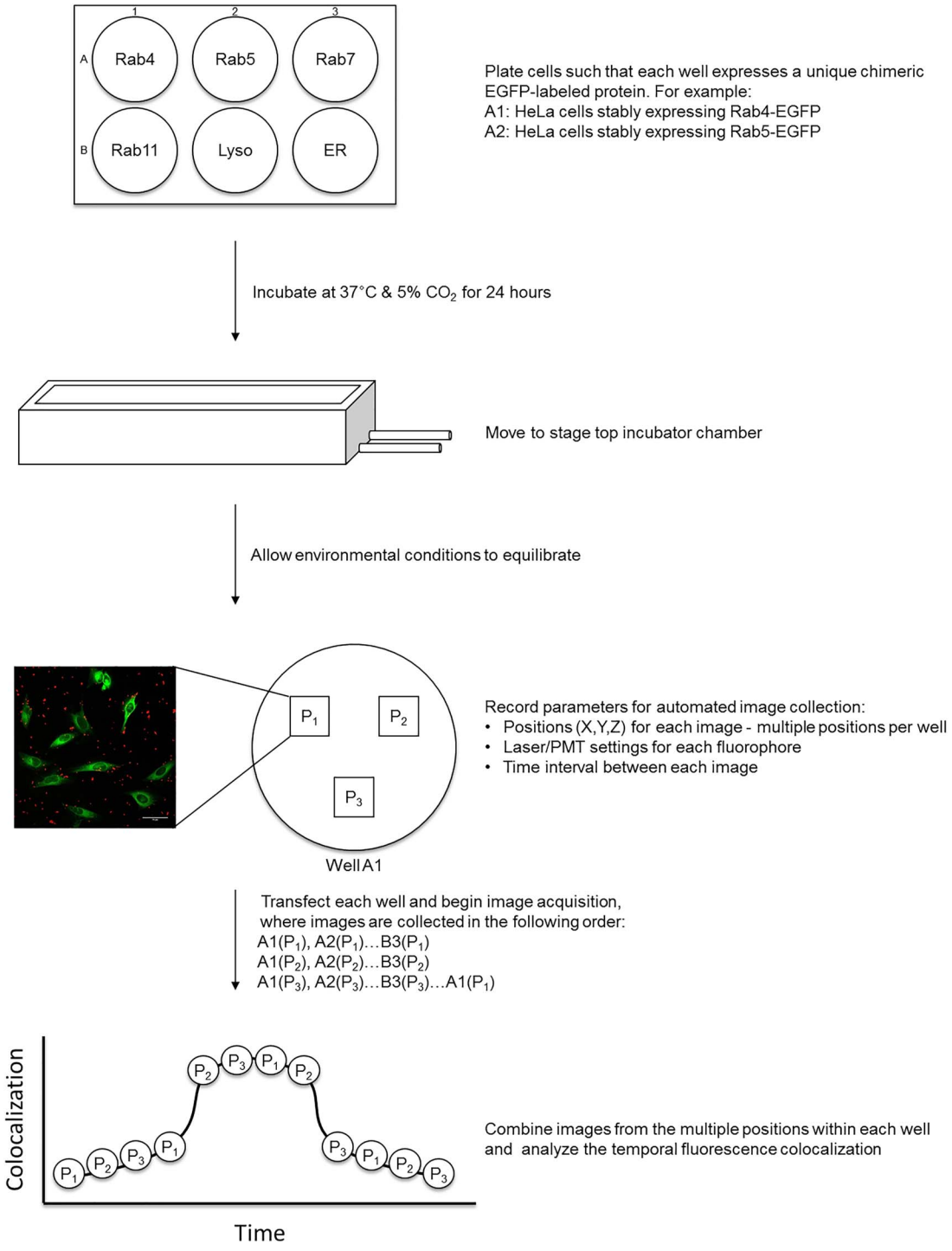

Fig. 1. Intracellular trafficking flowchart. A flow chart for tracking the intracellular localization of endocytosed molecules. Shown is the protocol for generating live-cell, kinetic colocalization profiles between the molecules and multiple intracellular locations.

function were maintained with a stage-top incubator equipped with temperature, humidity and CO_2 control. Automated stage controls were used to record and recall the exact X/Y coordinate of an image position, allowing multiple wells to be imaged in a single live-cell experiment. Nikon's Perfect Focus System (PFS) was used to prevent axial drift in the focal plane during long-term and multi-well imaging [9]. Finally, a dry objective was used to collect images across multiple wells/positions without continual application of liquid immersion media.

Fluorophores used in live-cell imaging are susceptible to photobleaching, depending on the sensitivity of the fluorophore and the frequency of image acquisition [10]. For our assay, intracellular organelles were labeled through the constitutive expression of fluorescent chimeric proteins, thereby minimizing photobleaching

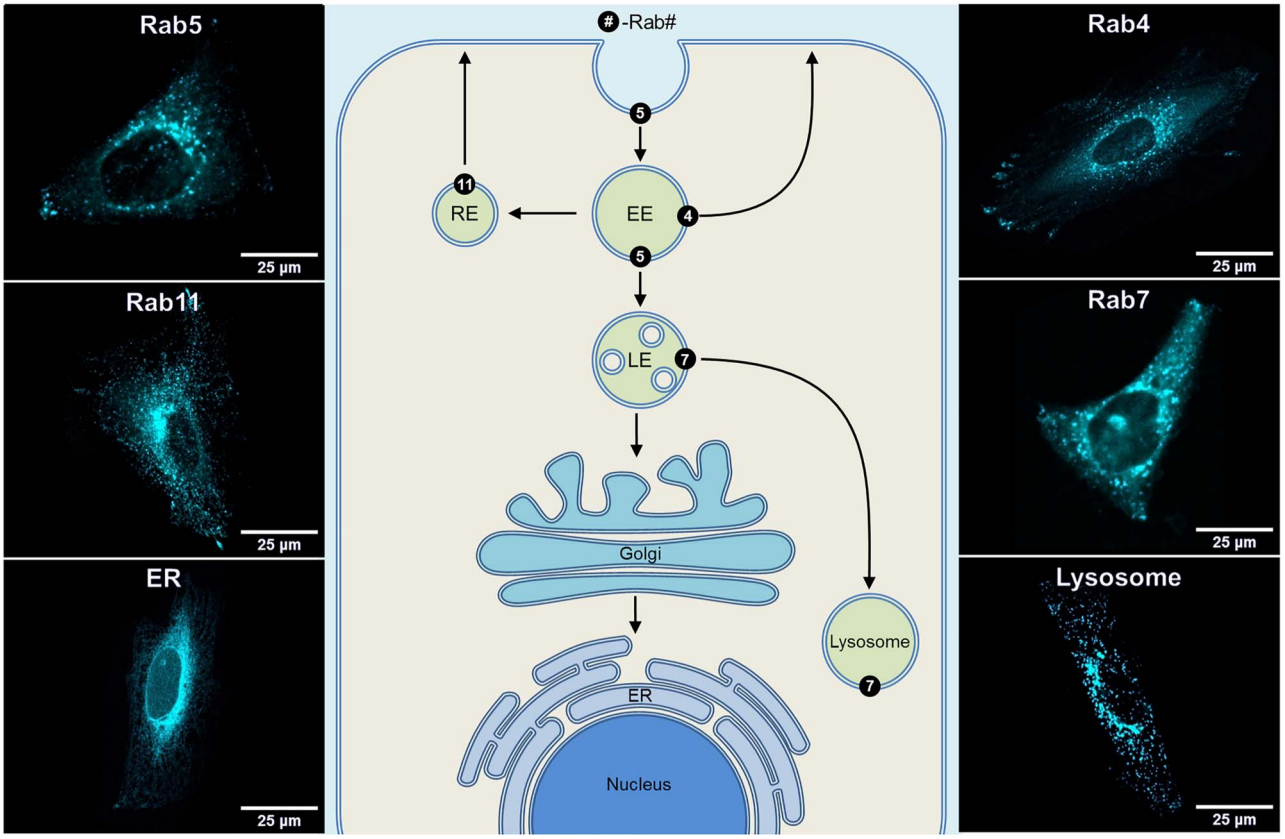

Fig. 2. Intracellular trafficking pathways in eukaryotic cells. To track the intracellular location of fluorescent molecules, HeLa cells were engineering to express EGFP-labeled proteins. Rab5 (5) facilitates receptor-mediated endocytosis and vesicle fusion with the EE. Rab4 (4) regulates fast endosomal recycling from the EE to the PM, and Rab11 (11) mediates slow endosomal recycling through the RE. Rab7 (7) directs trafficking and fusion of the LE with the lysosome. LAMP1 is used as a marker for the lysosome, and calreticulin as a marker for the ER.

through the continual supply of new fluorophores. Photobleaching of both the siRNA strands and organelles was further minimized by collecting images at multiple positions in each well. This allowed wells to be imaged at short intervals (~30 min) while the specific positions in each well were imaged at longer intervals (~1.5 h) (Fig. 1).

To characterize the kinetic association of siRNAs with intracellular locations common to endocytosis and intracellular trafficking, we engineered HeLa cells to express chimeric enhanced green florescent protein (EGFP) labeled proteins associated with intracellular trafficking: Rab4, Rab5, Rab7, Rab11, lysosomal associated membrane protein 1 (LAMP1) and calreticulin [(endoplasmic reticulum (ER)] (Fig. 2). Ras-like guanine triphosphatases (GTPases) (Rab) proteins, of which over 60+ members have been identified in humans, are associated with membrane trafficking [11]. Each Rab protein has distinct intracellular localization and trafficking through their association with motor, membrane and soluble N-ethylmaleimide-sensitive fusion protein attachment receptor (SNARE) proteins [11]. Endosomal membranes often contain multiple Rab proteins that promote sorting of contents to distinct regions of the membrane and trafficking to different intracellular destinations [12]. Rab5 is associated with the recycling endosome (RE) and endosomal maturation, but the majority of activated Rab5 is localized to the early endosome (EE) [13]. Rab4, also localized in the EE, regulates fast endosomal recycling from the EE to the plasma membrane (PM) [14]. Rab11 mediates slow endosomal recycling from the EE to an intermediate RE before trafficking to the PM [15]. Rab7 directs trafficking and fusion of the late endosome (LE) to the lysosome [16]. Endosomal maturation from EE to LE is characterized by a simultaneous increase in Rab7 and decrease in Rab5 [17]. LAMP1 is a transmembrane protein primarily residing in the lysosome [18]. Calreticulin is a calcium binder that resides in storage compartments of the ER [19].

In our previous work, we demonstrated that the activity of siRNAs was altered by the presence of dextran in the sNP delivery vehicles [20]. As both formulations of sNPs (with and without dextran) were capable of delivering siRNAs to cells (as quantified through flow cytometry), we hypothesized that the addition of dextran significantly altered the intracellular processing of the siRNAs. Here, we have investigated the kinetics of siRNA intracellular trafficking associated with delivery by sNPs +/−dextran over a ~24-h period. Images were collected at ~ 30 min intervals and then analyzed using the Pearson's correlation coefficient for the entire image (Fig. 3).

The kinetic association of each siRNA strand (guide and passenger) with Rab4-, Rab5- and Rab7-containing vesicles was similar, with rapid accumulation, retention and decay for siRNAs delivered by either sNP (Fig. 4). While siRNAs trafficked to Rab7 were unaffected by dextran functionalization, siRNAs delivered by the −dextran sNP had greater retention of the passenger strands in Rab4- and Rab5-containing vesicles than the guide strands. This would suggest that functionalizing sNPs with dextran alters the way siRNA strands are initially processed in fast/EEs (Rab4/5) but does not affect their subsequent trafficking to LEs (Rab7).

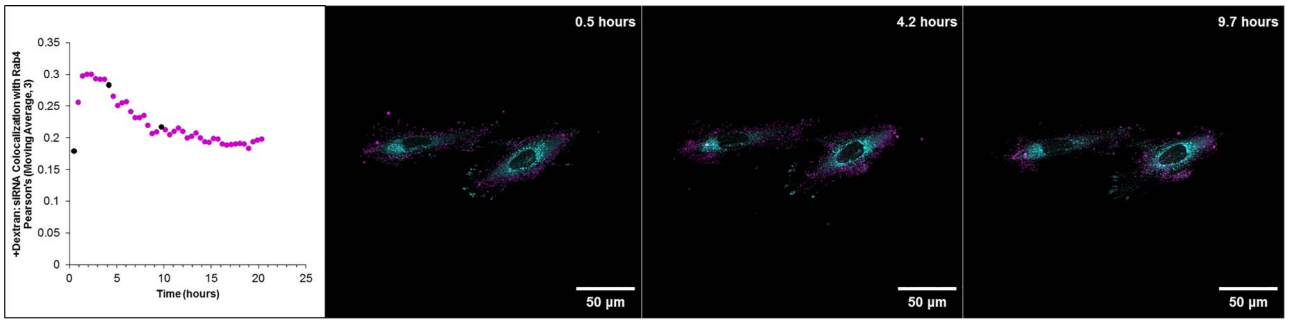

Fig. 3. Image analyses to determine kinetic colocalization profiles. Confocal images of HeLa cells expressing Rab4-GFP (cyan) transfected with sNPs +dextran and fluorescently labeled siRNAs (only guide strand fluorescence shown, magenta), taken at different time points post-transfection. Live cell images were collected at ~30 min intervals over a ~ 24-h period. Colocalization between the siRNA guide strand and Rab4 was calculated using Pearson's correlation coefficient. The increase in colocalization at 4.2 h relative to the other time points can be seen from the increased number of white pixels (overlap between cyan and magenta).

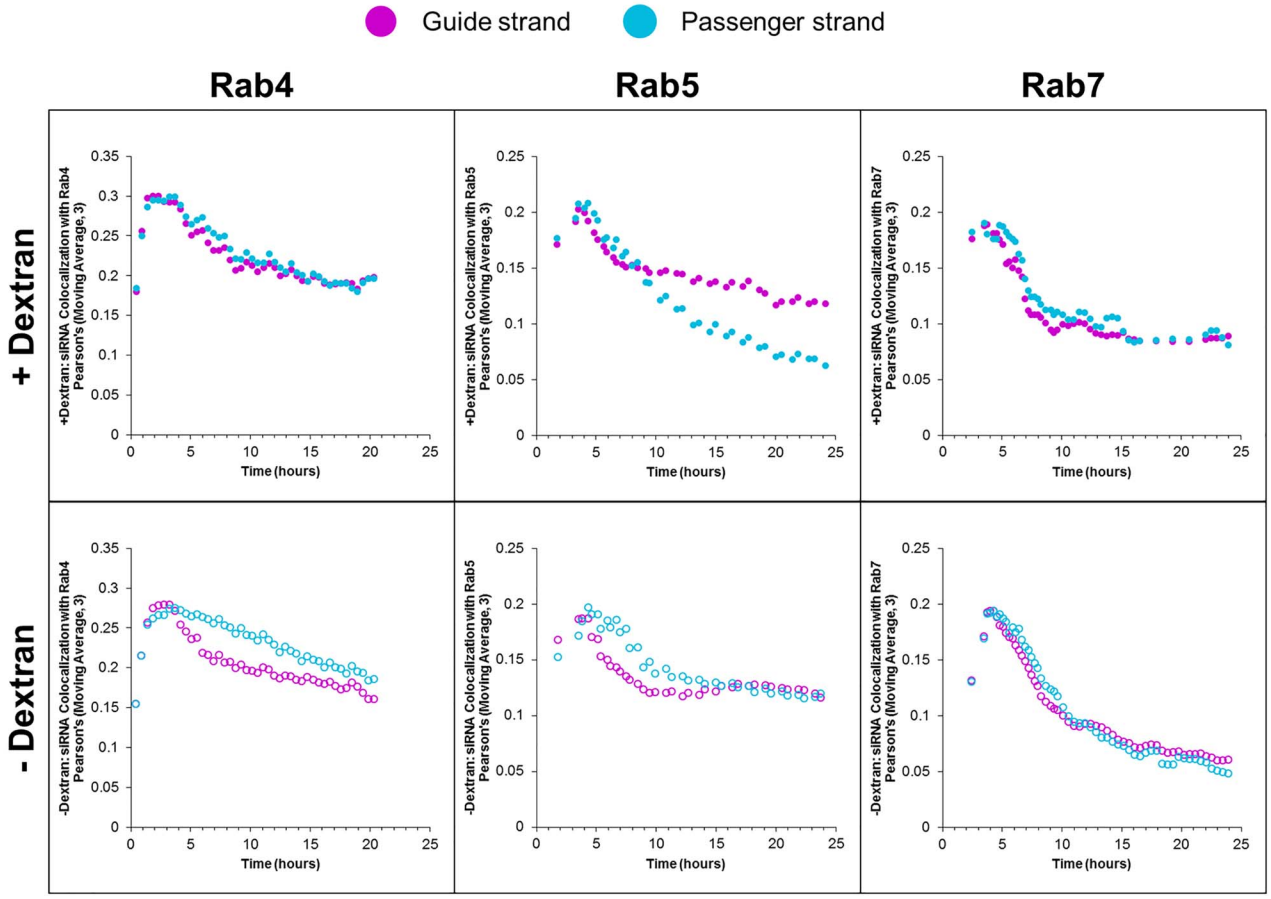

Fig. 4. Kinetic colocalization profiles of siRNA with Rab4, Rab5 and Rab7. Colocalization of siRNA strands, either guide (magenta) or passenger (cyan), with EGFP-labeled proteins. Following siRNA transfection by sNPs with (+) or without (−) dextran, live cell images were collected at ~30 min intervals for ~24 h. Colocalization between fluorophores was assessed using the Pearson's correlation coefficient of each image.

In Rab11-containing vesicles, the accumulation of passenger/guide strands was similar when delivered by sNPs −dextran, whereas siRNAs delivered by sNPs +dextran had greater accumulation of passenger strands than guide strands (Fig. 5). In the lysosome, there was little difference between the trafficking of siRNA strands when delivered by either sNP, however the rate of siRNA accumulation in the lysosome decreased over the duration of the experiment for sNPs +dextran, but increased for sNPs −dextran. The greatest difference in siRNA trafficking between sNPs was observed in the ER where siRNA strands delivered by sNPs −dextran were only briefly localized, whereas siRNA strands delivered by sNPs +dextran steadily accumulate over time.

Using the combined data sets of intracellular localization, we determined the intracellular pathway used by each siRNA strand and compared the differences between delivery by the different sNPs (Fig. 6). Initially, siRNAs rapidly accumulate in the EE and colocalize

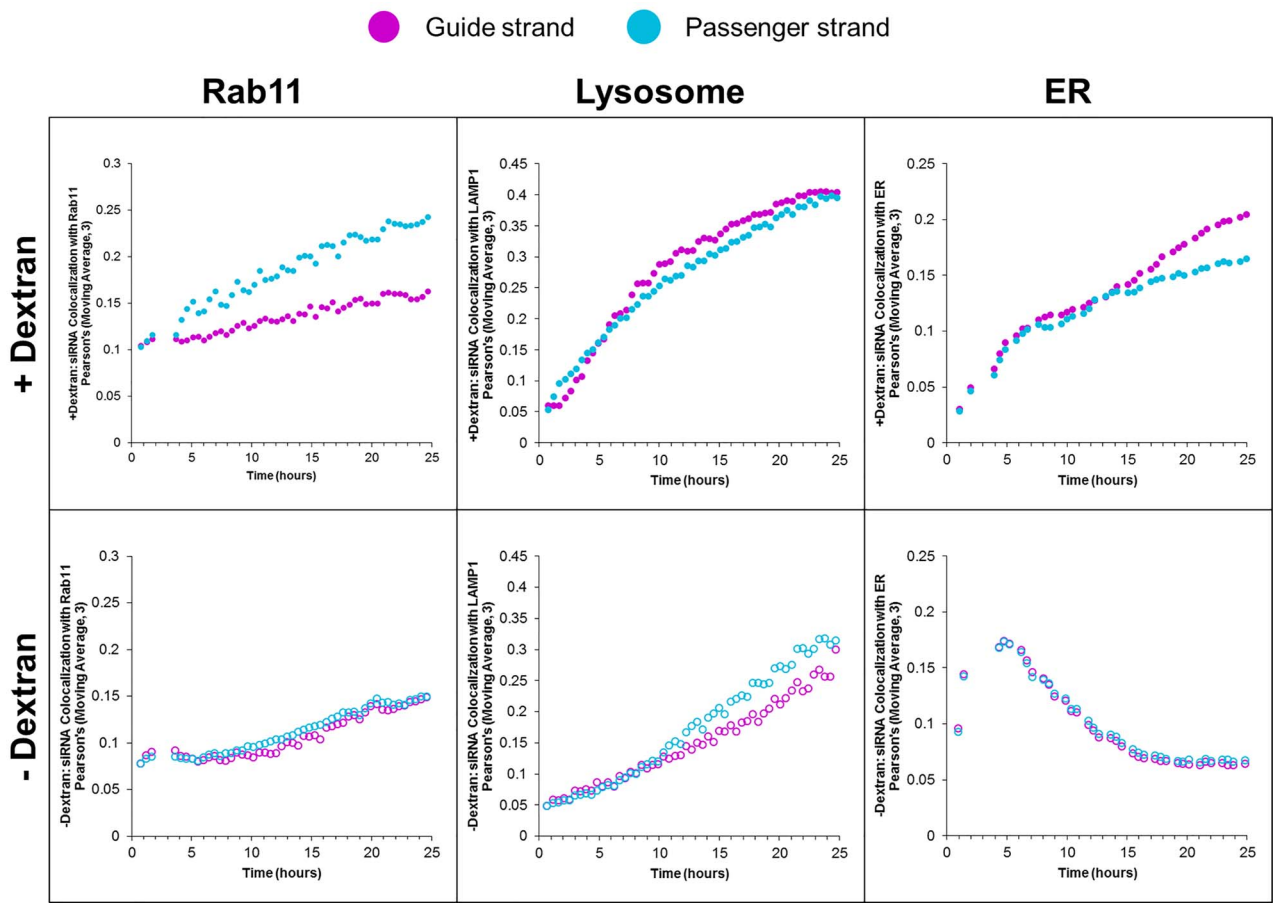

Fig. 5. Kinetic colocalization profiles of siRNA with Rab11, lysosome and ER. Colocalization of siRNA strands, either guide (magenta) or passenger (cyan), with EGFP-labeled proteins stably expressed in HeLa cells. Following siRNA transfection, using sNPs functionalized either with (+) or without (−) dextran, live cell images were collected using a confocal microscope at ~30 min intervals for ~24 h. Colocalization between fluorophores was assessed using the Pearson's correlation coefficient of each image.

to regions associated with fast endosomal recycling (Rab4) and endosomal maturation (Rab5/7). Variations in siRNA strand trafficking are observed, with greater retention of the passenger strand than the guide strand in Rab5 vesicles. After the EE, siRNAs began to accumulate in lysosomes, REs (Rab11) and the ER. The primary distinction in siRNA trafficking between sNPs +/−dextran occurred in the ER, where siRNA colocalization diminishes over time for sNPs −dextran but increases for sNPs +dextran. Further, the accumulation and retention of the passenger strand was biased toward fast endosomal recycling when delivered using sNPs −dextran but slow endosomal recycling when using sNPs +dextran.

Discussion

Here, we have described an automated method that increases the throughput of confocal microscopy for analyzing the trafficking of endocytosed material. Comparing the kinetic colocalization profiles of guide and passenger siRNAs, this assay was capable of detecting changes in colocalization across multiple intracellular locations and methods of delivery. This was specifically evident in Rab5-positive vesicles, where passenger strands had a longer residence time than their guide strand counterparts.

Using sNPs with and without dextran, we identified differences in the ways siRNAs were trafficked that correlated with silencing. In the ER, siRNAs delivered by sNPs +dextran accumulated over a 24-h period. Conversely, siRNAs delivered by sNPs −dextran reached peak colocalization 3 h post-transfection, with their association decaying exponentially afterwards. As the ER is a nucleation site for siRNA-mediated RNAi, these findings may explain why dextran functionalization of sNPs enhances the silencing activity of delivered siRNAs [21].

Combining our data sets across multiple intracellular locations, we determined the intracellular pathways taken by each siRNA strand and identified differences caused by the properties of the delivery vehicle. As observed in the trafficking of the sense strand, dextran functionalization of sNPs reduced fast endosomal recycling (Rab4) and increased slow endosomal recycling (Rab11). For both siRNA strands, dextran functionalization of the sNPs prolonged intracellular retention, which was evident in the EE (Rab5), the ER and the lysosome. The same methods could be applied to other siRNA delivery vehicles to improve the understanding of the intracellular events leading to successful siRNA delivery.

This proof-of-concept study showed promising differences in the trafficking of siRNAs based on their delivery vehicle. As this study was limited to HeLa cells, future studies should be conducted in other cell types to determine the extent that cell type effects the trafficking of endocytosed cargo. In this study, colocalization was determined using entire images; subsequent studies should explore colocalization

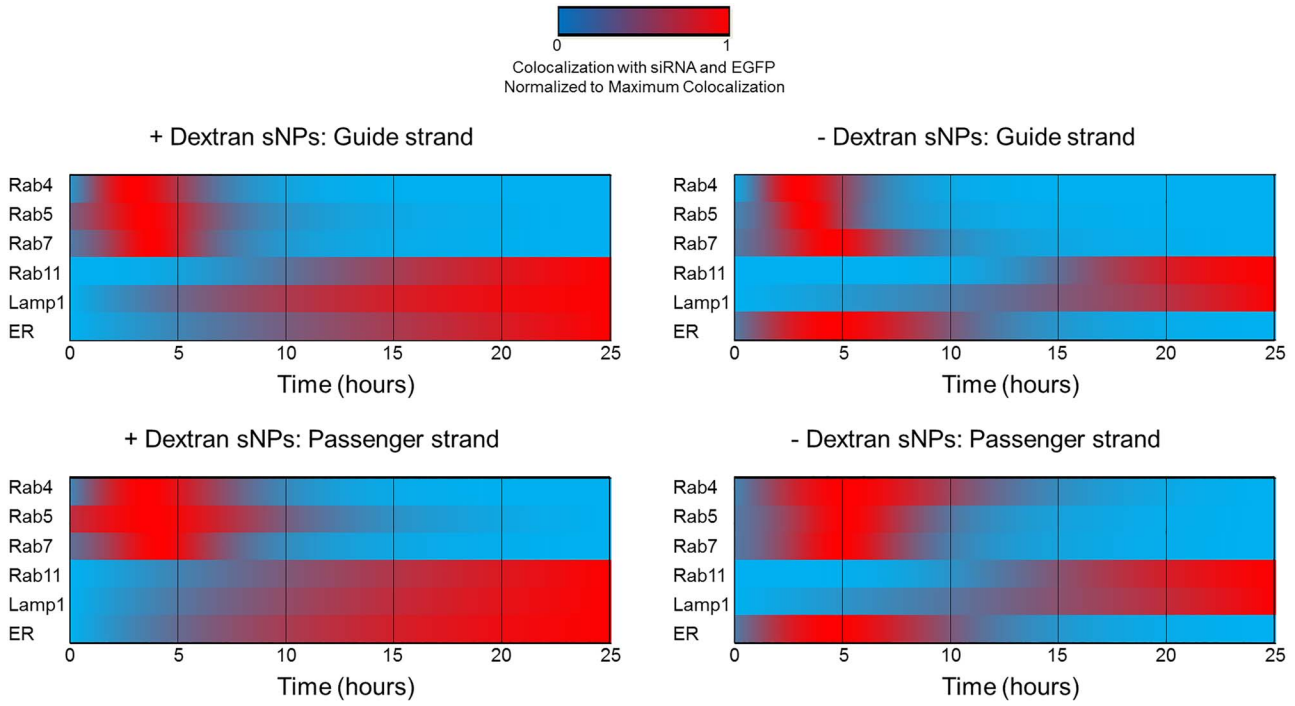

Fig. 6. Kinetic colocalization heat maps. Heat maps generated from the colocalization profiles between siRNA strands and the corresponding organelles (Figs 4 and 5).

on a single cell basis, as this could provide insight into the differences in intracellular trafficking across the cell population.

This assay is beneficial to studying of the impact of the characteristics of delivery vehicles on siRNA trafficking and activity. However, there is considerable potential for further optimization, by expanding the scope of the assay to include additional intracellular pathways and organelles. Further, we believe that the findings presented demonstrate the potential applications of this assay to a variety of cellular processes involving the intracellular transport of therapeutic cargo, such as DNA, mRNA, small molecules and peptides.

Materials and methods

Materials

See Supplementary Table 1 for a detailed list of reagents and solutions.

Cell lines

HeLa cells constitutively expressing EGFP-labeled proteins Rab5 and Rab7 were generously provided by Matthew Seaman (University of Cambridge). HeLa cells constitutively expressing EGFP-labeled proteins (Rab4, Rab11, LAMP1 and calreticulin) were generated using published methods [22]. Briefly, cells were seeded in 6-well plates and transfected 24 h post-seeding with 10 µL Lipofectamine 2000 (LF2K) and 4 µg of one of the following plasmids: pEGFP-C1 RAB11A (Rab11), pEGFP-C1-RAB4b (Rab4), pEGFP-ER-14 (ER) or pEGFP-N3-LAMP1 (lysosome). Three days post-transfection, cells were sorted and re-plated according to their EGFP expression using a flow cytometer. This process was repeated at 7 and 14 days post-transfection. The average EGFP expression of the final population was analyzed over several cell cycles and found to be stable. All cell lines were maintained in antibiotic-free Dulbecco's Modified Eagle Medium (DMEM) supplemented with 10% fetal bovine serum (FBS). Cells were incubated at 37°C in 5% CO_2, at 100% relative humidity, and subcultured every 4–5 days by trypsinization.

Transfection and intracellular trafficking

HeLa cells constitutively expressing an EGFP-labeled protein (Rab4, Rab5, Rab7, Rab11, calreticulin and LAMP1) were seeded in 15-well confocal plates at a density of 1000 cells/well and cultured in antibiotic-free growth media (DMEM+FBS). Twenty-four hours after seeding, cells were transferred to a stage-top incubator chamber and incubated at 37°C, 5% CO_2 and 100% relative humidity. The X, Y and Z positions were recorded for three locations in each well. Cells were then treated with 10 µL of transfection solution containing Opti-MEM, siRNA and sNPs, yielding final concentrations of 100 nM siRNA and 200 µg/mL sNP. After verifying the X, Y, and Z positions in each well, images were collected at ~30 min intervals over ~24 h. Cell morphology was monitored for signs of cytotoxicity, which was not observed at any time.

Image acquisition and analysis

Images were acquired on a Nikon A1 confocal laser scanning microscope using a Nikon Plan Fluor 40×/.75 dry objective. EGFP (488/530) fluorescence was measured using an excitation of 488 nm with a multi-line Argon laser. Each siRNA duplex was labeled at the 3′ end of the guide and passenger strand, which has been shown to have no effect on siRNA activity [23]. Q570 (560/595) fluorescence (siRNA guide strand) was excited at 560 nm by a HeNe laser. Q670 (647/700) fluorescence (siRNA passenger strand) was excited at 647 nm by a HeNe laser. As per the manufacturer's information, the Q570 and Q670 dyes are functionally equivalent to Cy3 and

Cy5, respectively, and insensitive to changes in pH [24,25], making them useful for tracking the siRNA strands even in endolysosomal vesicles. The focal plane for each image was chosen to maximize EGFP fluorescence intensity, which should be the focal plane through the middle of the cells, and was maintained using the Nikon PFS.

Images were acquired sequentially as single XY images using two-count Line Kalman averaging. Each well was imaged at its first position prior to returning to the first well and then imaging the second position in each well. After acquiring images at three positions in each well, the sequence began again at the first position in the first well. Using this imaging approach minimized photobleaching while also minimizing the time between images for a given well. The entire image was used to determine the Pearson's correlation coefficient for each fluorophore pairing. Images were analyzed in batch through Fiji [26] using the Bio-Formats and JACoP plugins [27].

Supplementary data

Supplementary data mentioned in the text are available to subscribers in *JMICRO* online.

Funding

This work was supported by Michigan State University; the National Science Foundation [CBET1510895, 1547518, 1802992]; and the National Institutes of Health [GM089866].

Acknowledgements

We would like to thank the members of the Cellular and Biomolecular Laboratory for their advice and support. We thank Dr. Melinda Frame and the Michigan State University Center for Advanced Microscopy for support of our confocal microscopy experiments.

Conflict of interest

The authors declare no competing financial interests.

References

1. Shu Y, Pi F, Sharma A, Rajabi M, Haque F, Shu D, Leggas M, Evers B M, and Guo P (2014) Stable RNA nanoparticles as potential new generation drugs for cancer therapy. *Adv. Drug Deliv. Rev.* 66: 74–89.
2. Sahay G, Querbes W, Alabi C, Eltoukhy A, Sarkar S, Zurenko C, Karagiannis E, Love K, Chen D, Zoncu R, Buganim Y, Schroeder A, Langer R, and Anderson D G (2013) Efficiency of siRNA delivery by lipid nanoparticles is limited by endocytic recycling. *Nat. Biotechnol.* 7: 653–658.
3. Setten R L, Rossi J J, and Han S (2019) The current state and future directions of RNAi-based therapeutics. *Nat. Rev. Drug Discov.* 6: 421–446.
4. Watson P, Jones A T, and Stephens D J (2005) Intracellular trafficking pathways and drug delivery: Fluorescence imaging of living and fixed cells. *Adv. Drug Deliv. Rev.* 57: 43–61.
5. Vermeulen L M P, Brans T, De Smedt S C, Remaut K, and Braeckmans K (2018) Methodologies to investigate intracellular barriers for nucleic acid delivery in non-viral gene therapy. *Nano Today* 21: 74–90.
6. Hirsch M, and Helm M (2015) Live cell imaging of duplex siRNA intracellular trafficking. *Nucleic Acids Res.* 9: 4650–4660.
7. Shukla R S, Jain A, Zhao Z, and Cheng K (2016) Intracellular trafficking and exocytosis of a multi-component siRNA nanocomplex. *Nanomed. Nanotechnol. Biol. Med.* 5: 1323–1334.
8. Gilleron J, Querbes W, Zeigerer A, Borodovsky A, and Marsico G (2013) Image-based analysis of lipid nanoparticle-mediated siRNA delivery, intracellular trafficking and endosomal escape. *Nat. Biotechnol.* 7: 638–646.
9. Peters J (2008) Nikon instruments TiE-PFS dynamic focusing system. *Nat. Methods | Appl Notes*.
10. Claxton N S, Fellers T J, and Davidson M W (2006) Laser scanning confocal microscopy. *Encycl Med Devices Instrum* 21: 1–37.
11. Hutagalung A H, and Novick P J (2011) Role of Rab GTPases in membrane traffic and cell physiology. *Physiol. Rev.* 1: 119–149.
12. Stenmark H (2009) Rab GTPases as coordinators of vesicle traffic. *Nat. Rev. Mol. Cell Biol.* 8: 513–525.
13. Sönnichsen B, De Renzis S, Nielsen E, Rietdorf J, and Zerial M (2000) Distinct membrane domains on endosomes in the recycling pathway visualized by multicolor imaging of Rab4, Rab5, and Rab11. *J. Cell Biol.* 4: 901–913.
14. McCaffrey M W, Bielli A, Cantalupo G, Mora S, Roberti V, Santillo M, Drummond F, and Bucci C (2001) Rab4 affects both recycling and degradative endosomal trafficking. *FEBS Lett.* 495: 21–30.
15. Hales C M, Vaerman J P, and Goldenring J R (2002) Rab11 family interacting protein 2 associates with myosin Vb and regulates plasma membrane recycling. *J. Biol. Chem.* 277: 50415–50421.
16. Jordens I, Fernandez-Borja M, Marsman M, Dusseljee S, Janssen L, Calafat J, Janssen H, Wubbolts R, and Neefjes J (2001) The Rab7 effector protein RILP controls lysosomal transport by inducing the recruitment of dynein-dynactin motors. *Curr. Biol.* 11: 1680–1685.
17. Rojas R, Van Vlijmen T, Mardones G A, Prabhu Y, Rojas A L, Mohammed S, A J R H, Raposo G, Van Der Sluijs P, and Bonifacino J S (2008) Regulation of retromer recruitment to endosomes by sequential action of Rab5 and Rab7. *J. Cell Biol.* 183: 513–526.
18. Eskelinen E L (2006) Roles of LAMP-1 and LAMP-2 in lysosome biogenesis and autophagy. *Mol. Aspects Med.* 27: 495–502.
19. Krause K, and Michalak M (1997) Calreticulin. *Cell* 88: 439–443.
20. Vocelle D, Chesniak O M, Malefyt A P, Comiskey G, Adu-Berchie K, Smith M R, Chan C, and Walton S P (2016) Dextran functionalization enhances nanoparticle-mediated siRNA delivery and silencing. *Technology (Singap World Sci)*. 4: 42–54.
21. Stalder L, Heusermann W, Sokol L, Trojer D, Wirz J, Hean J, Fritzsche A, Aeschimann F, Pfanzagl V, Basselet P, Weiler J, Hintersteiner M, Morrissey D V, and Meisner-Kober N C (2013) The rough endoplasmatic reticulum is a central nucleation site of siRNA-mediated RNA silencing. *EMBO J.* 8: 1115–1127.
22. Kaufman W L, Kocman I, Agrawal V, Rahn H-P, Besser D, and Gossen M (2008) Homogeneity and persistence of transgene expression by omitting antibiotic selection in cell line isolation. *Nucleic Acids Res.* 17: e111–e111.
23. Berezhna S Y, Supekova L, Supek F, Schultz P G, and Deniz A A (2006) siRNA in human cells selectively localizes to target RNA sites. *Proc. Natl. Acad. Sci. U. S. A.* 20: 7682–7687.
24. Carter T, Reddington M, and Biosearch Technologies (2014) Cyanine dyes. US 8.436,153 B2.
25. Matsumoto B (2002) Cell biological applications of confocal microscopy. *Methods Cell Biol.* 70: 321.
26. Schindelin J, Arganda-Carreras I, Frise E, Kaynig V, Longair M, Pietzsch T, Preibisch S, Rueden C, Saalfeld S, Schmid B, Tinevez J Y, White D J, Hartenstein V, Eliceiri K, Tomancak P, and Cardona A (2012) Fiji: An open-source platform for biological-image analysis. *Nat. Methods* 7: 676–682.
27. Bolte S, and Cordelières F P (2006) A guided tour into subcellular colocalization analysis in light microscopy. *J. Microsc.* 3: 213–232.